

See discussions, stats, and author profiles for this publication at: <https://www.researchgate.net/publication/262608109>

Mesoporous Amorphous FePO₄ Nanospheres as High-Performance Cathode Material for Sodium-Ion Batteries

ARTICLE *in* NANO LETTERS · MAY 2014

Impact Factor: 13.59 · DOI: 10.1021/nl501152f · Source: PubMed

CITATIONS

38

READS

37

6 AUTHORS, INCLUDING:



[Yongjin Fang](#)

Wuhan University

7 PUBLICATIONS 43 CITATIONS

[SEE PROFILE](#)



[Jiangfeng Qian](#)

Wuhan University

34 PUBLICATIONS 1,505 CITATIONS

[SEE PROFILE](#)

Mesoporous Amorphous FePO₄ Nanospheres as High-Performance Cathode Material for Sodium-Ion Batteries

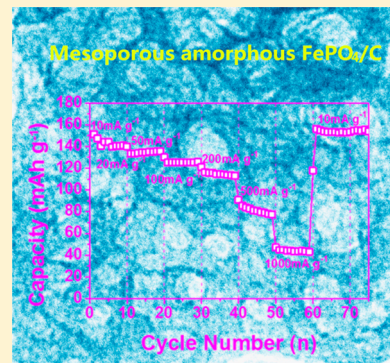
Yongjin Fang,[†] Lifen Xiao,^{*,‡} Jiangfeng Qian,[†] Xinping Ai,[†] Hanxi Yang,[†] and Yuliang Cao^{*,†}

[†]Hubei Key Laboratory of Electrochemical Power Sources, College of Chemistry and Molecular Sciences, Wuhan University, Wuhan 430072, China

[‡]College of Chemistry, Central China Normal University, Wuhan 430079, China

Supporting Information

ABSTRACT: FePO₄ nanospheres are synthesized successfully through a simple chemically induced precipitation method. The nanospheres present a mesoporous amorphous structure. Electrochemical experiments show that the FePO₄/C electrode demonstrates a high initial discharging capacity of 151 mAh g⁻¹ at 20 mA g⁻¹, stable cyclability (94% capacity retention ratio over 160 cycles), as well as high rate capability (44 mAh g⁻¹ at 1000 mA g⁻¹) for Na-ion storage. The superior electrochemical performance of the FePO₄/C nanocomposite is due to its particular mesoporous amorphous structure and close contact with the carbon framework, which significantly improve the ionic and electronic transport and intercalation kinetics of Na ions.



KEYWORDS: FePO₄, amorphous, mesoporous structure, Na-ion batteries

Sodium ion batteries (SIBs) have recently been pursued actively as the most attractive alternative to lithium ion batteries (LIBs) for the application of large-scale energy storage, because of their evident advantages, such as low cost, environmental benignity, and wide availability of sodium.^{1–3} To realize SIB technology, a crucial issue is to discover applicable Na ion host materials. Because the ionic radius of Na is much larger than that of Li,^{4–6} it is a great challenge to find out materials to accommodate sufficient Na ions, as well as to ensure rapid and reversible Na ion insertion/extraction. Recently, a large number of compounds, such as transition metal oxides,^{7–13} phosphates,^{14–16} ferrocyanide,^{17–19} hard carbon,^{20,21} and metal alloys,^{22–27} have been investigated as cathode or anode materials for SIBs. Some compounds have exhibited good reversible capacity and cycling stability, demonstrating a feasibility of SIB technology. However, from the ecological and environmental point of view some rare elements, such as Ni, Co, V, and so on, are not suitable to be used for electrode materials in the case of large-scale energy storage. Fe element, otherwise, is earth-abundant and much less expensive. Thus, Fe-based materials have motivated great attention of being developed as low-cost and safe cathode materials for SIBs.

Among Fe-based cathode materials, iron phosphate compounds^{28–31} are mostly investigated, especially NaFePO₄,^{32–36} Na₂FeP₂O₇,^{37–40} and FePO₄.⁴¹ As an analogue to LiFePO₄, NaFePO₄ has been surveyed early as cathode material for SIBs.^{32,36} NaFePO₄ is reported to have two phases: the maricite and olivine phases.^{32,34,35} Maricite NaFePO₄ is a thermody-

namically stable phase and can be directly prepared by the traditional solid-state synthesis method, while it shows electrochemical sluggishness due to its frustrated ionic channels in the structure.^{34,35} In contrast, olivine NaFePO₄ shows remarkable electrochemical reversibility for Na ion storage,^{32,36} while it can only be acquired by chemical or electrochemical redox reaction of olivine LiFePO₄.^{33,42} Na₂FeP₂O₇ adopts a triclinic structure and has large Na ion migration channels but only shows a low reversible capacity of 82 mAh g⁻¹.^{37,39} In short, crystalline iron phosphates have so far exhibited unsatisfactory Na ion storage performance, because the lattice frameworks either can only provide undersized channel for Na ion diffusion or lack available sites for Na ions to reside. To address these problems, amorphous structure seems to be an effective resort, because there will be less structural confinement to the insertion/extraction reaction of the large sized Na ions in the amorphous framework.

Among the iron phosphate compounds, FePO₄ is easy to form an amorphous phase, for example, using a simple precipitation process at low temperature.^{43–45} Amorphous FePO₄ has been reported as a cathode material for LIBs, showing high reversible capacity (175 mAh g⁻¹) and stable cyclability.^{44,46–49} Besides, the amorphous FePO₄ demonstrates a monotonous potential change owing to a single-phase Li ion insertion/extraction reaction, which is favorable to the control

Received: March 28, 2014

Revised: May 18, 2014

Published: May 23, 2014



of the charging/discharging stages of the practical battery. These advantages have also attracted considerable interest to use the amorphous FePO_4 as a Na ion host. Shiratsuchi et al reported an amorphous FePO_4 with a reversible Na ion storage capacity of 146 mAh g^{-1} at a rate of 0.1 mA cm^{-2} and suggested that the Na ion intercalation sites in FePO_4 were the same as that of Li ions.⁵⁰ Zhao et al. synthesized monodisperse iron phosphate nanospheres through a solvent extraction route, which gave a reversible Na ion storage capacity of 108 mAh g^{-1} at 0.025C (3.5 mA g^{-1}).⁵¹ Also, Liu et al. reported porous amorphous FePO_4 nanoparticles connected by single-wall carbon nanotubes as cathode material for Na ion batteries, which showed a reversible capacity of 120 mAh g^{-1} at 10 mA g^{-1} with excellent cycling stability.⁴¹ However, this reversible capacity (120 mAh g^{-1}) is much lower than the theoretical capacity (178 mAh g^{-1}) of FePO_4 , indicating that there is still a large improving margin in the capacity and rate capacity. Herein, we report a facile synthesis of mesoporous amorphous FePO_4 nanospheres and the application as the cathode material for SIBs. The mesoporous structures are conducive to the full infiltration of the electrolyte, reducing the migrating distance of Na ions, facilitating Na ions exchange across the interfaces, and tolerating the large volume change of the electrodes during the Na ions insertion/extraction, so as to greatly enhance the Na ion storage kinetics and structural stability.⁴⁶

The mesoporous amorphous FePO_4 nanospheres were synthesized through a simple chemically induced precipitation method. First, iso-concentrational $\text{NH}_4\text{H}_2\text{PO}_4$ and $(\text{NH}_4)_2\text{Fe}(\text{SO}_4)_2$ reacted to form a colloid solution. Then H_2O_2 was added to form light yellow precipitate. The precipitate precursor was subsequently calcined to obtain the mesoporous amorphous FePO_4 . To improve the conductivity, the mesoporous amorphous FePO_4 was ball-milled with a conductive carbon (Ketjen Black) into a well-dispersed FePO_4/C composite. Figure 1a displays a thermogravimetric (TG) curve of the FePO_4 hydrate precursor. The weight loss took place mainly below 200°C and terminated at about 400°C .

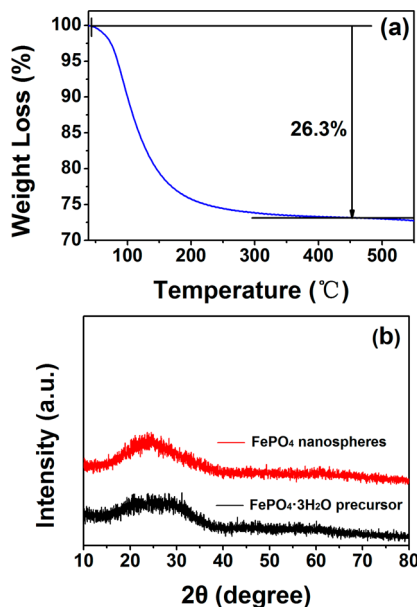


Figure 1. (a) Thermal analysis of the $\text{FePO}_4 \cdot 3\text{H}_2\text{O}$ precursor and (b) the XRD patterns of the $\text{FePO}_4 \cdot 3\text{H}_2\text{O}$ precursor and the FePO_4 nanospheres.

$^\circ\text{C}$, which should be attributed to the dehydration process of the precursor. The total weight loss is observed to be 26.3%, indicating that the stoichiometric ratio of FePO_4 and H_2O is 1:3. The TG result suggests that the FePO_4 hydrate precursor is $\text{FePO}_4 \cdot 3\text{H}_2\text{O}$, which is consistent with previous work.^{45,52} Figure 1b shows the X-ray diffraction (XRD) patterns of the $\text{FePO}_4 \cdot 3\text{H}_2\text{O}$ precursor before and after calcination in air at 400°C . Both of the XRD patterns show no signals of crystalline diffraction peaks, namely, demonstrate an amorphous characteristic. The energy dispersive X-ray spectroscopy (EDS) mapping analysis (see Supporting Information Figure S1) shows that the amorphous FePO_4 calcinated at 400°C is composed of Fe (6.92, 6.26, and 0.59 keV), P (1.90 keV), and O (0.42 keV) elements with a P/Fe atomic ratio of ca. 1.16, again confirms that the calcined product is FePO_4 .

The scanning electron microscopic (SEM) image (Figure 2a) shows that the as prepared FePO_4 has a spherelike morphology

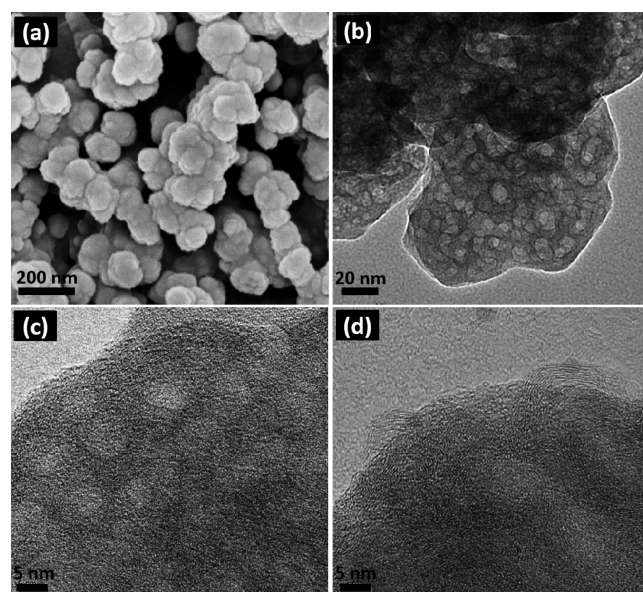


Figure 2. Morphological analysis of the FePO_4 nanospheres and the FePO_4/C composite: (a) SEM image of the FePO_4 nanospheres; (b) TEM image of the FePO_4 nanospheres; (c) HRTEM image of the FePO_4 nanospheres; and (d) HRTEM image of the FePO_4/C composite.

with a diameter of about 100 nm. A rough surface also can be observed. The transmission electron microscope (TEM) was further performed to examine the morphology of FePO_4 . As shown in Figure 2b and Supporting Information Figure S2, there are a lot of small pores dispersed in each nanosphere. The pore size was observed to be about 10 nm from the high-resolution TEM image (Figure 2c), indicating the existence of a mesoporous structure. The Brunauer–Emmett–Teller (BET) measurement (Supporting Information Figure S3) also confirms a mesoporous structure, as the nitrogen adsorption and desorption isotherms present a type IV curve with a type III hysteresis loop (IUPAC classification).⁵³ On the basis of the BET analysis, the mesoporous FePO_4 nanospheres have a surface area as high as $19.33 \text{ m}^2 \text{ g}^{-1}$. Besides, The HRTEM image (Figure 2c) also shows an amorphous nature because no discernible lattice fringe can be observed. Even after being ball-milled with carbon, the mesoporous nanospheric structure of FePO_4 remained untouched (Supporting Information Figure

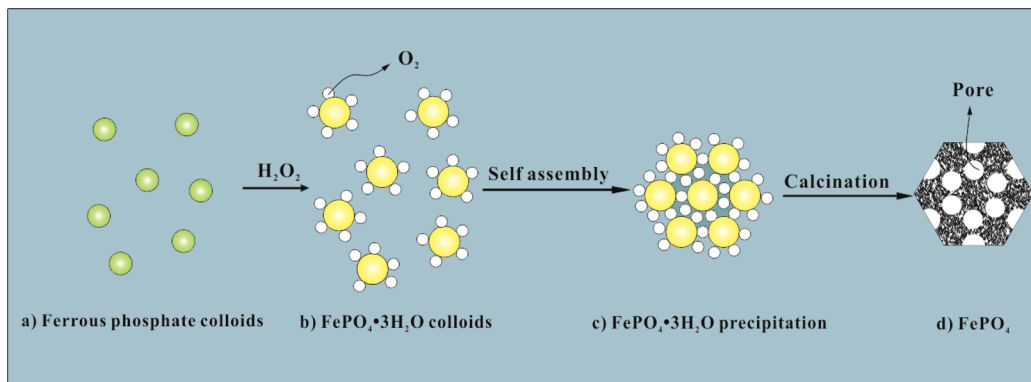


Figure 3. An illustration of the formation mechanism of the mesoporous FePO_4 nanospheres.

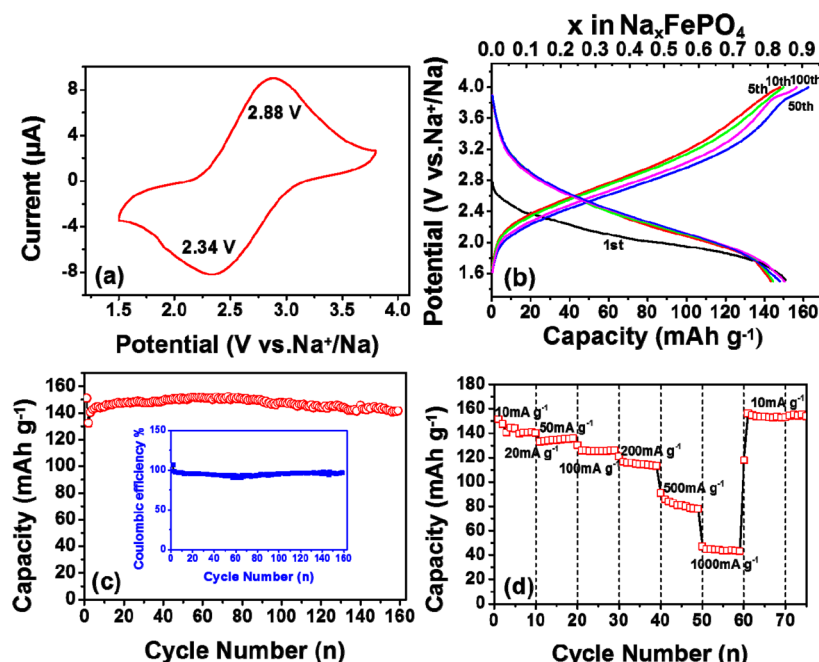


Figure 4. Electrochemical characterization of the FePO_4/C cathode: (a) CV curve conducted at a scan rate of 0.1 mV s^{-1} (voltage window $1.5\text{--}3.8 \text{ V}$); (b,c) galvanostatic discharging/charging profiles performed at a current density of 20 mA g^{-1} and the corresponding cycling performance; and (d) rate capability. The counter electrode was a Na disk and the electrolyte was $1.0 \text{ mol L}^{-1} \text{NaPF}_6$ dissolved in an EC/DEC solution (EC/DEC = 1:1 by vol), voltage window was $1.5\text{--}4.0 \text{ V}$.

S2c). Figure 2d shows the HRTEM image of the mesoporous FePO_4/C composite. As can be clearly observed, the surface of the amorphous FePO_4 nanospheres are tightly covered by a layer of graphite-structured carbon, which constructs an electronic conducting matrix surrounding the FePO_4 nanoparticles. This structure should be beneficial to the electrochemical utilization and rate capability of the FePO_4/C nanocomposite.

Because of its limited penetration depth of the incident laser into the samples, Raman spectroscopic analysis is extremely sensitive to the surface species and can exactly detect the chemical signal in the surface region. The Raman spectra of FePO_4 and the FePO_4/C composite are presented in Supporting Information Figure S4. As can be seen, the two Raman spectra are totally different. In the case of FePO_4 , two peaks near 620 and 1020 cm^{-1} can be observed and are assigned to the intramolecular stretching modes of the PO_4^{3-} anion.⁴⁷ In contrast, in the case of the FePO_4/C composite the two peaks located at 1355 and 1605 cm^{-1} are unambiguously

associated with the D (disordered carbon, sp^3) band and the G band (graphite, sp^2) of Raman vibration modes for amorphous carbon, respectively.⁵⁴ No response from FePO_4 can be detected, indicating that FePO_4 was fully covered by carbon. As is well-known, the peak intensity ratio (I_D/I_G) is indexed to the degree of disordering of carbon. The I_D/I_G ratio in Supporting Information Figure S4 is calculated to be 0.93, reflecting a relatively high level of graphitization of the carbon coating. Thus, the Raman spectroscopic evidence corroborates that FePO_4 can be successfully covered by carbon by facile ball-milling method. The carbon coating should be able to provide effective electric connection between the particles.⁵⁵

In order to better understand the formation of the mesoporous amorphous FePO_4 nanospheres, a possible mechanism is proposed as illustrated in Figure 3. First, $\text{NH}_4\text{H}_2\text{PO}_4$ reacted with $(\text{NH}_4)_2\text{Fe}(\text{SO}_4)_2$ to form ferrous phosphate hydrate colloids (Figure 3a), which was confirmed by a typical Tyndall effect (as shown in Supporting Information Figure S5). Then, when H_2O_2 was introduced, the $\text{Fe}(\text{II})$ ions

were chemically oxidized to Fe(III) ions and turned into less soluble iron phosphate hydrate. Meanwhile, the newly generated Fe(III) ions also promoted the decomposition of H₂O₂ to O₂, which absorbed on the surface of the FePO₄ hydrate colloids (Figure 3b). Under vigorous stirring, the FePO₄ hydrate colloids with adsorbed oxygen preferred to aggregate and self-assemble into the spherical FePO₄ hydrate nanoparticles to reduce the free energy of the system (Figure 3c). Subsequently, some voids in-between the FePO₄ nanoparticles were left behind to form the mesoporous structure under high temperature (Figure 3d). Therefore, the chemically induced precipitation process makes the colloidal particles self-assemble into the mesoporous FePO₄ nanospheres.

Figure 4 displays the Na ion storage performance of the as-prepared FePO₄/C composite. The cyclic voltammogram (CV) curve shows a pair of current peaks positioned respectively at 2.88 and 2.34 V (Figure 4a), corresponding to the redox of Fe(III)/Fe(II). The broad redox peaks imply a continuous single-phase redox reaction, which is quite different from that of the olivine FePO₄ characterized by a biphasic transition during the sodiation/desodiation.³⁶ Figure 4b shows the charging-discharging voltage profiles of the FePO₄/C cathode at different cycles at a current rate of 20 mA g⁻¹. The profiles exhibit a monotonous voltage change, agreeing well with the observation in the CV plot (Figure 4a). As mentioned above, the voltage slopes during charging and discharging could be beneficial for easy controlling the state of the charging and discharging during battery operation. The electrode delivered an initial discharge and charge capacities of 151 and 141 mAh g⁻¹, respectively, corresponding to a Coulombic efficiency of 107% in the first cycle. The initial discharge capacity is about 85% of the theoretical capacity of FePO₄ (178 mAh g⁻¹), much higher than those of FePO₄ nanoparticles reported previously.^{41,50,51} The improved performance of the as-prepared FePO₄/C composite probably benefits from the optimized treatment temperature, small particle size, tight carbon coating, and mesoporous structure. The discharging profiles of the as-prepared FePO₄/C nanocomposite almost overlapped in the subsequent cycles (Figure 4b), exhibiting excellent electrochemical reversibility. After 160 cycles, the FePO₄/C electrode still delivered a reversible capacity of 142 mAh g⁻¹, corresponding to a capacity retention ratio of 94% (Figure 4c). The rate capability of the amorphous FePO₄/C nanocomposite was also evaluated to investigate its feasibility for high power applications (Figure 4d). As can be seen, the electrode shows a reversible capacity of 135, 126, 115, 80, and 44 mAh g⁻¹ at 50, 100, 200, 500, and 1000 mA g⁻¹, respectively, which is much superior to that (50 mAh g⁻¹ at 100 mA g⁻¹) of the previous report.⁴¹ When the current density returned back to 10 mA g⁻¹, a capacity of 154 mAh g⁻¹ still was recovered. These results are indicative of excellent rate capability and electrochemical reversibility of the FePO₄/C nanocomposite for Na ion storage.

To understand the effect of carbon coating on the electrochemical performance, the bare mesoporous amorphous FePO₄ nanospheres were also investigated and their electrochemical performance is given in Supporting Information Figure S5. The bare FePO₄ electrode exhibited a similar discharging/charging behavior to the FePO₄/C composite. However, the initial discharging capacity is only 130 mAh g⁻¹ at the current density of 20 mA g⁻¹ (Supporting Information Figure S6a), lower than that of the FePO₄/C composite (Figure 4b). Besides, the discharging capacity faded rapidly

with cycling and was only 40 mAh g⁻¹ after 160 cycles (Supporting Information Figure S6b). When discharged at a moderate current density of 100 mA g⁻¹, only a reversible capacity of 31 mAh g⁻¹ was obtained (Supporting Information Figure S6c). Such poor cycling performance and rate capability of the bare FePO₄ electrode imply that the coating carbon played a critical role on the excellent electrochemical performance of the FePO₄/C nanocomposite. It could act as a conductive bridge to provide a fast and continuous electron transport pathway so as to greatly facilitate the reaction kinetics of the electrode.

To further explore the Na ion insertion mechanism, ex situ XRD was performed to characterize the phase changes of the FePO₄/C electrode at full charging and discharging status. As demonstrated in Supporting Information Figure S7, no new phase emerges in both XRD patterns at the complete discharging to 1.5 V and subsequent charging to 4.0 V, namely that the FePO₄/C electrode stays in an amorphous state throughout the whole discharging and charging processes. This structural consistency could effectively buffer the huge volumetric change during the insertion/extraction of the large-sized Na ions so as to sustain the high cycling stability of the electrode.

The above electrochemical characterization demonstrates that the FePO₄/C composite manifests excellent performance considering the high reversible capacity, cyclability, and rate capability, relating to the peculiar structure of itself. The mesoporous structure not only facilitates the infiltration of electrolyte inside the material to construct fast diffusion pathways for Na ions in liquid and solid phases but also provides a large electrochemical reaction interface, which would extremely decrease the electrochemical polarization and improve the capacity utilization as well as rate capability of the electrode. The carbon tightly covered on the surface of the nanoparticles forms a good conductive framework, which greatly improves the electric conductivity of the whole electrode. Moreover, the amorphous nature of FePO₄ can avoid the lattice stress and provide continuous Na ion diffusion pathways and insertion sites, so as to greatly improve the reversible capacity and structural stability.

In conclusion, mesoporous amorphous FePO₄ nanospheres were synthesized by a simple chemically induced precipitation method. The as-prepared FePO₄/C composite exhibited a high initial discharging capacity of 151 mAh g⁻¹ at 20 mA g⁻¹, stable cyclability (94% capacity retention ratio over 160 cycles) as well as high rate capability (44 mAh g⁻¹ at 1000 mA g⁻¹). To the best of our knowledge, this is the first time such a high-performance FePO₄ material is reported for Na ion storage. The outstanding electrochemical features of the FePO₄/C composite are attributed to its particular mesoporous, amorphous structure and close contact with the carbon framework, which significantly improve the ionic and electronic transport and intercalation kinetics of Na ions. This work also presents a novel method for tailoring the structure of materials to enhance their electrochemical performance for energy storage devices such as batteries and supercapacitors.

ASSOCIATED CONTENT

Supporting Information

Experimental details, material characterizations, EDS spectrum of the FePO₄ nanospheres, TEM images of the FePO₄ nanospheres, Raman spectra of the FePO₄ and FePO₄/C, a typical Tyndall effect, N₂ adsorption/desorption isotherms of

the FePO₄ nanospheres, electrochemical characterization of the FePO₄ cathode, and ex situ XRD patterns of the FePO₄/C cathodes. This material is available free of charge via the Internet at <http://pubs.acs.org>.

AUTHOR INFORMATION

Corresponding Authors

*(Y.C.) E-mail: ylcao@whu.edu.cn. Phone: +86-027-68754526.
*(L.X.) E-mail: lfxiao@mail.ccnu.edu.cn.

Notes

The authors declare no competing financial interest.

ACKNOWLEDGMENTS

We thank financial support by the National Science Foundation of China (Nos. 21373155, 21333007).

REFERENCES

- (1) Slater, M. D.; Kim, D.; Lee, E.; Johnson, C. S. *Adv. Funct. Mater.* **2013**, *23*, 947–958.
- (2) Ellis, B. L.; Nazar, L. F. *Curr. Opin. Solid State Mater. Sci.* **2012**, *16*, 168–177.
- (3) Pan, H.; Hu, Y.-S.; Chen, L. *Energy Environ. Sci.* **2013**, *6*, 2338–2360.
- (4) Kim, S.-W.; Seo, D.-H.; Ma, X.; Ceder, G.; Kang, K. *Adv. Energy Mater.* **2012**, *2*, 710–721.
- (5) Shao, Y.; Xiao, J.; Wang, W.; Engelhard, M.; Chen, X.; Nie, Z.; Gu, M.; Saraf, L. V.; Exarhos, G.; Zhang, J.-G.; Liu, J. *Nano Lett.* **2013**, *13*, 3909–3914.
- (6) Hwang, T. H.; Jung, D. S.; Kim, J.-S.; Kim, B. G.; Choi, J. W. *Nano Lett.* **2013**, *13*, 4532–4538.
- (7) Cao, Y.; Xiao, L.; Wang, W.; Choi, D.; Nie, Z.; Yu, J.; Saraf, L. V.; Yang, Z.; Liu, J. *Adv. Mater.* **2011**, *23*, 3155–3160.
- (8) Ding, J. J.; Zhou, Y. N.; Sun, Q.; Yu, X. Q.; Yang, X. Q.; Fu, Z. W. *Electrochim. Acta* **2013**, *87*, 388–396.
- (9) Hamani, D.; Ati, M.; Tarascon, J.-M.; Rozier, P. *Electrochim. Commun.* **2011**, *13*, 938–941.
- (10) Gu, M.; Kushima, A.; Shao, Y.; Zhang, J.-G.; Liu, J.; Browning, N. D.; Li, J.; Wang, C. *Nano Lett.* **2013**, *13*, 5203–5211.
- (11) Oh, S.-M.; Myung, S.-T.; Yoon, C. S.; Lu, J.; Hassoun, J.; Scrosati, B.; Amine, K.; Sun, Y.-K. *Nano Lett.* **2014**, *14*, 1620–1626.
- (12) Wang, Y.; Yu, X.; Xu, S.; Bai, J.; Xiao, R.; Hu, Y. S.; Li, H.; Yang, X. Q.; Chen, L.; Huang, X. *Nat. Commun.* **2013**, *4*, 2365.
- (13) Yu, X.; Pan, H.; Wan, W.; Ma, C.; Bai, J.; Meng, Q.; Ehrlich, S. N.; Hu, Y. S.; Yang, X. Q. *Nano Lett.* **2013**, *13*, 4721–4727.
- (14) Jian, Z.; Zhao, L.; Pan, H.; Hu, Y.-S.; Li, H.; Chen, W.; Chen, L. *Electrochim. Commun.* **2012**, *14*, 86–89.
- (15) Park, S. I.; Gocheva, I.; Okada, S.; Yamaki, J.-i. *J. Electrochem. Soc.* **2011**, *158*, A1067–A1070.
- (16) Oh, S.-M.; Myung, S.-T.; Hassoun, J.; Scrosati, B.; Sun, Y.-K. *Electrochim. Commun.* **2012**, *22*, 149–152.
- (17) Qian, J.; Zhou, M.; Cao, Y.; Ai, X.; Yang, H. *Adv. Energy Mater.* **2012**, *2*, 410–414.
- (18) Wang, L.; Lu, Y.; Liu, J.; Xu, M.; Cheng, J.; Zhang, D.; Goodenough, J. B. *Angew. Chem., Int. Ed.* **2013**, *52*, 1964–1967.
- (19) Wessells, C. D.; Huggins, R. A.; Cui, Y. *Nat. Commun.* **2011**, *2*, 550.
- (20) Cao, Y.; Xiao, L.; Sushko, M. L.; Wang, W.; Schwenzer, B.; Xiao, J.; Nie, Z.; Saraf, L. V.; Yang, Z.; Liu, J. *Nano Lett.* **2012**, *12*, 3783–3787.
- (21) Kuratani, K.; Yao, M.; Senoh, H.; Takeichi, N.; Sakai, T.; Kiyobayashi, T. *Electrochim. Acta* **2012**, *76*, 320–325.
- (22) Xiao, L.; Cao, Y.; Xiao, J.; Wang, W.; Kovarik, L.; Nie, Z.; Liu, J. *Chem. Commun.* **2012**, *48*, 3321–3323.
- (23) Qian, J.; Chen, Y.; Wu, L.; Cao, Y.; Ai, X.; Yang, H. *Chem. Commun.* **2012**, *48*, 7070–7072.
- (24) Wu, L.; Hu, X.; Qian, J.; Pei, F.; Wu, F.; Mao, R.; Ai, X.; Yang, H.; Cao, Y. *Energy Environ. Sci.* **2014**, *7*, 323–328.
- (25) Qian, J.; Xiong, Y.; Cao, Y.; Ai, X.; Yang, H. *Nano Lett.* **2014**, *14*, 1865–1869.
- (26) Han, X.; Liu, Y.; Jia, Z.; Chen, Y.-C.; Wan, J.; Weadock, N.; Gaskell, K. J.; Li, T.; Hu, L. *Nano Lett.* **2013**, *14*, 139–147.
- (27) Wang, J. W.; Liu, X. H.; Mao, S. X.; Huang, J. Y. *Nano Lett.* **2012**, *12*, 5897–5902.
- (28) Padhi, A. K.; Nanjundaswamy, K. S.; Goodenough, J. B. *J. Electrochem. Soc.* **1997**, *144*, 1188–1194.
- (29) Nishimura, S.; Kobayashi, G.; Ohoyama, K.; Kanno, R.; Yashima, M.; Yamada, A. *Nat. Mater.* **2008**, *7*, 707–711.
- (30) Kang, B.; Ceder, G. *Nature* **2009**, *458*, 190–193.
- (31) Cao, Y.; Xiao, L.; Sushko, M. L.; Wang, W.; Schwenzer, B.; Xiao, J.; Nie, Z.; Saraf, L. V.; Yang, Z.; Liu, J. *Nano Lett.* **2012**, *12*, 3783–3787.
- (32) Oh, S.-M.; Myung, S.-T.; Hassoun, J.; Scrosati, B.; Sun, Y.-K. *Electrochim. Commun.* **2012**, *22*, 149–152.
- (33) Moreau, P.; Guyomard, D.; Gaubicher, J.; Boucher, F. *Chem. Mater.* **2010**, *22*, 4126–4128.
- (34) Zaghib, K.; Trottier, J.; Hovington, P.; Brochu, F.; Guerfi, A.; Mauger, A.; Julien, C. M. *J. Power Sources* **2011**, *196*, 9612–9617.
- (35) Sun, A.; Manivannan. *J. Electrochim. Soc. Trans.* **2011**, *35*, 3–7.
- (36) Zhu, Y.; Xu, Y.; Liu, Y.; Luo, C.; Wang, C. *Nanoscale* **2013**, *5*, 780–787.
- (37) Kim, H.; Shakoor, R. A.; Park, C.; Lim, S. Y.; Kim, J.-S.; Jo, Y. N.; Cho, W.; Miyasaka, K.; Kahraman, R.; Jung, Y.; Choi, J. W. *Adv. Funct. Mater.* **2013**, *23*, 1147–1155.
- (38) Barpanda, P.; Liu, G.; Ling, C. D.; Tamaru, M.; Avdeev, M.; Chung, S.-C.; Yamada, Y.; Yamada, A. *Chem. Mater.* **2013**, *25*, 3480–3487.
- (39) Barpanda, P.; Ye, T.; Nishimura, S.-i.; Chung, S.-C.; Yamada, Y.; Okubo, M.; Zhou, H.; Yamada, A. *Electrochim. Commun.* **2012**, *24*, 116–119.
- (40) Chen, C.-Y.; Matsumoto, K.; Nohira, T.; Hagiwara, R.; Oriksa, Y.; Uchimoto, Y. *J. Power Sources* **2014**, *246*, 783–787.
- (41) Liu, Y.; Xu, Y.; Han, X.; Pellegrinelli, C.; Zhu, Y.; Zhu, H.; Wan, J.; Chung, A. C.; Vaaland, O.; Wang, C.; Hu, L. *Nano Lett.* **2012**, *12*, 5664–5668.
- (42) Casas-Cabanas, M.; Roddatis, V. V.; Saurel, D.; Kubiak, P.; Carretero-González, J.; Palomares, V.; Serras, P.; Rojo, T. *J. Mater. Chem.* **2012**, *22*, 17421–17423.
- (43) Kim, H.; Kim, S.-W.; Hong, J.; Lim, H.-D.; Kim, H. S.; Yoo, J.-K.; Kang, K. *J. Electrochim. Soc.* **2011**, *158*, A930–A935.
- (44) Prosini, P. P.; Lisi, M.; Scaccia, S.; Carewska, M.; Cardellini, F.; Pasquali, M. *J. Electrochim. Soc.* **2002**, *149*, A297–A301.
- (45) Xiao, Y.; Pu, W.; Wan, W.; Cui, Y. *Int. J. Electrochim. Sci.* **2013**, *8*, 938–948.
- (46) Yin, Y.; Hu, Y.; Wu, P.; Zhang, H.; Cai, C. *Chem. Commun.* **2012**, *48*, 2137–2139.
- (47) Kim, S. W.; Ryu, J.; Park, C. B.; Kang, K. *Chem. Commun.* **2010**, *46*, 7409–7411.
- (48) Guo, C. X.; Shen, Y. Q.; Dong, Z. L.; Chen, X. D.; Lou, X. W.; Li, C. M. *Energy Environ. Sci.* **2012**, *5*, 6919–6922.
- (49) Okada, S.; Yamamoto, T.; Okazaki, Y.; Yamaki, J.-i.; Tokunaga, M.; Nishida, T. *J. Power Sources* **2005**, *146*, 570–574.
- (50) Shiratsuchi, T.; Okada, S.; Yamaki, J.; Nishida, T. *J. Power Sources* **2006**, *159*, 268–271.
- (51) Zhao, J.; Jian, Z.; Ma, J.; Wang, F.; Hu, Y. S.; Chen, W.; Chen, L.; Liu, H.; Dai, S. *ChemSusChem* **2012**, *5*, 1495–500.
- (52) Boonchom, B.; Danvirutai, C. *Ind. Eng. Chem. Res.* **2007**, *46*, 9071–9076.
- (53) Sing, K. S. W.; Everett, D. H.; Haul, R. H. W.; Moscou, L.; Pierotti, R. A.; Rouquerol, J.; Siemieniewska, T. *Pure Appl. Chem.* **1985**, *57*, 603–619.
- (54) Yoshikawa, M.; Katagiri, G.; Ishida, H.; Ishitani, A.; Ono, M.; Matsumura, K. *Appl. Phys. Lett.* **1989**, *55*, 2608–2610.
- (55) Zheng, Z.; Wang, Y.; Zhang, A.; Zhang, T.; Cheng, F.; Tao, Z.; Chen, J. *J. Power Sources* **2012**, *198*, 229–235.